

# AWM 4 and MKW 4 - two very different poor clusters observed with XMM-Newton

Ewan O'Sullivan<sup>1</sup> and J. M. Vrtilek<sup>1</sup>

<sup>1</sup> *Harvard-Smithsonian Center for Astrophysics*

We present observations of two poor clusters, AWM 4 and MKW 4, observed by XMM-Newton. Both systems are relaxed, with little substructure evident in their X-ray halos or galaxy populations. However, their temperature structures are markedly different, with AWM 4 isothermal to the resolution of the EPIC instruments while MKW 4 shows a strong decline in temperature towards the core. Metal abundance also increases more strongly in the core of MKW 4 than AWM 4. Three dimensional models show further differences, suggesting that gas in the core of AWM 4 has been heated and has expanded outwards. The dominant elliptical galaxy of AWM 4 hosts an AGN with large-scale radio jets, while the central cD of MKW 4 shows no current AGN activity. We therefore conclude that the difference in activity cycle of the AGN in the two galaxies is responsible for the difference in IGM properties between the two clusters.

## 1. Introduction

MKW 4 and AWM 4 are fairly relaxed poor clusters, originally identified in the Morgan et al. (1975) and Albert et al. (1977) surveys. Each is dominated by a giant elliptical or cD galaxy, surrounded by  $\sim 50$  (MKW 4) or  $\sim 30$  (AWM 4) other galaxies. Kinematic studies of the galaxy populations of the two clusters show them to be fairly evenly distributed about their mean redshifts, with no sign of significant substructure (Koranyi & Geller 2002). Both clusters are morphologically segregated, with absorption line systems found predominantly toward the center of each system.

The dominant galaxies of MKW 4 and AWM 4 are NGC 4073 and NGC 6051 respectively. Both are highly luminous and  $\sim 1.5$  magnitudes brighter than the second ranked galaxy in their clusters. NGC 4073 shows evidence of a past merger. It has a kinematically decoupled core (Fisher et al. 1995) and the spectroscopic age of the stellar population is  $\sim 7.5$  Gyr (Terlevich & Forbes 2002). It is the larger of the two galaxies, with  $\log L_B = 11.01 L_\odot$ . NGC 6051 hosts an active nucleus, revealed by a large scale radio feature extending from the galaxy core. The central point source is not detected at other wavelengths, which suggests that the axis of the AGN jets is in the plane of the sky and that the central engine is highly absorbed. The optical luminosity of NGC 6051 is  $L_B = 10.76 L_\odot$ .

Both clusters have been the subject of previous X-ray observations with *Einstein*, *ASCA* and *ROSAT*, all of which have shown them to be relaxed systems (dell'Antonio et al. 1995; Jones & Forman 1999) reasonably well modeled by at most two beta models (Helsdon & Ponman 2000; Finoguenov et al. 2001). The X-ray halo of MKW 4 has a mean temperature of  $\sim 1.7$  keV, and radial temperature profiles show that the temperature increases from  $\sim 1.3$  keV in the core to a peak above 2.5 keV at  $\sim 115$  kpc before dropping back to a

fairly constant temperature of  $\sim 1.5$  keV at higher radii. The *ASCA* data have been used to produce radial abundance profiles which show Fe, Si and S abundances which fall from central values of  $0.4\text{--}0.7 Z_\odot$  to  $0\text{--}0.2 Z_\odot$  at a radius of 500 kpc (Finoguenov et al. 2000). The halo of AWM 4 is somewhat simpler, having a relatively isothermal temperature profile out to a radius of at least  $\sim 200$  kpc. The mean temperature of the gas is  $\sim 2.5$  keV.

Given their relatively relaxed and undisturbed state, and the large mass concentrations associated with their central galaxies, these clusters are potentially excellent sites in which to observe cooling at the low end of the cluster mass range. We have used two *XMM-Newton* observations to study the structure of their X-ray halos, and in particular to determine whether they currently host cooling flows. Throughout these proceedings we assume  $H_0 = 75 \text{ km s}^{-1} \text{Mpc}^{-1}$  and normalise optical luminosities to the B-band luminosity of the sun  $L_{B\odot} = 5.2 \times 10^{32} \text{ erg s}^{-1}$ . MKW 4 lies at a redshift of  $z = 0.020$ , AWM 4 at  $z = 0.032$ , and we therefore assume distances to the two clusters of 80 Mpc and 127 Mpc respectively.

## 2. Results

MKW 4 was observed with *XMM-Newton* during orbit 373 (2001 December 21) in two exposures of  $\sim 16,000$  and  $\sim 4,500$  seconds. AWM 4 was observed during orbit 573 (2003 January 25-26) for just over 20,000 seconds. In both cases the EPIC MOS and PN instruments were operated in full frame and extended full frame modes respectively, with the medium filter. A detailed summary of the *XMM-Newton* mission and instrumentation can be found in Jansen et al. (2001), and references therein. The raw data from the EPIC instruments for the longer of the two exposures were processed with the publicly released version of the *XMM-Newton* Science Analysis System (SAS v.5.3.3 for MKW 4, SAS v.5.4.1 for AWM 4), using the EPCHAIN and EMCHAIN tasks. After filtering for bad pixels and columns, X-ray events corresponding

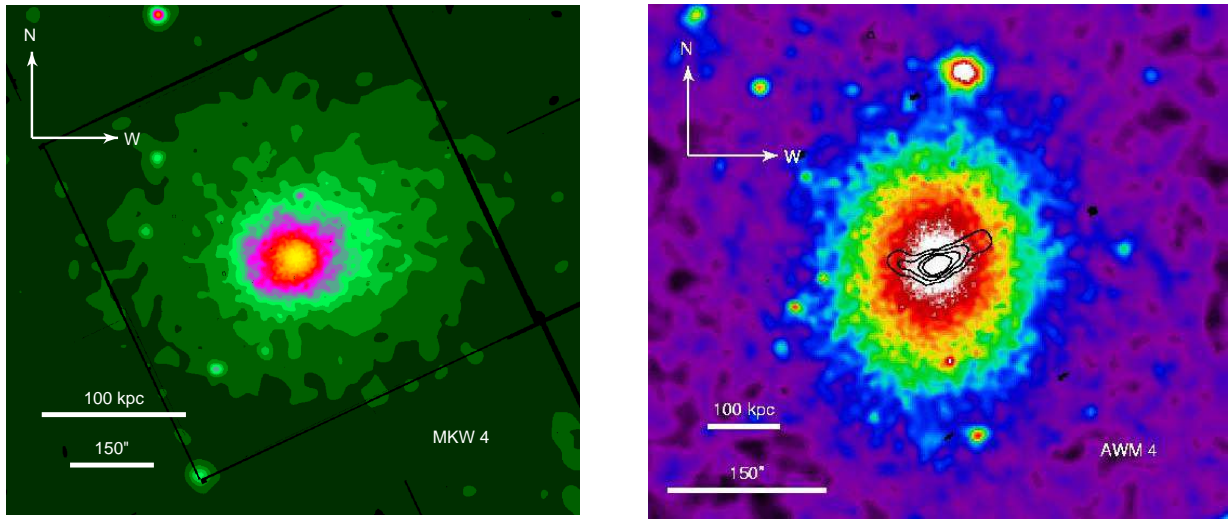


FIG. 1.— Adaptively smoothed X-ray images of MKW 4 (left) and AWM 4 (right). Radio contours, taken from the VLA First 20cm survey, are shown in black on the image of AWM 4. The bright source to the north of the AWM 4 cluster is a background QSO.

to patterns 0-12 for the two MOS cameras and patterns 0-4 for the PN camera were accepted. Investigation of the total count rate for the field revealed a short background flare at the beginning of the MKW 4 observation and another in the second half of the AWM 4 observation. Times when the total count rate deviated above the mean by more than  $3\sigma$  were therefore excluded. The effective exposure times for the MOS and PN cameras were 14.1 and 10.5 ksec in the case of MKW 4 and 17.4 and 12.7 ksec in the case of AWM 4. Images and spectra were extracted from the cleaned events lists with the SAS task EVSELECT. Figure 1 shows adaptively smoothed images of the two clusters.

### 2.1. Surface brightness profiles

In order to model the surface brightness distributions of the two clusters, we produced images for use in the CIAO SHERPA fitting software. Using data from all three EPIC cameras we searched for and removed all point sources, with the exception of false identifications associated with the cluster cores. We also generated background images based on the blank-sky data of Lumb (2002) and Read & Ponman (2003), and the telescope closed data of Marty et al. (2002), using the ‘double subtraction’ technique (Arnaud et al. 2002; Pratt et al. 2001). As the images contain many pixels with few (or zero) counts, we used the Cash statistic (Cash 1979) to perform the fits.

AWM 4 was reasonably well fit by two beta models, a more extended elliptical component and a circular central component. The parameters (and  $1\sigma$  errors) of the best fit model are shown in Table 1. Errors for each model were estimated with all fitted parameters free for perturbation. Position angle is measured anti-clockwise from north.

We initially attempted to model MKW 4 using either a single or two-component beta model, but this was unsuccessful. We decided instead to model sectors of the halo individually. We selected four sectors, covering the ma-

jor and minor axes of the halo. The NW and SE sectors showed deviations from a simple beta model, with the NW sector showing emission extending to higher radii, and the SE sector showing a ‘bulge’ of excess emission at  $\sim 20$  kpc. The two remaining sectors were well described by a single beta model and had similar core radii and slopes, leading us to fit them together. Taking into account the effect of the PSF and excluding all data outside the NE and SW sectors, we found the best fit to be a beta model with parameters as shown in Table 1. Note that this model is by necessity circular, with the axis ratio fixed at 1.0.

### 2.2. Temperature and Abundance profiles

In order to examine the large scale temperature and abundance structure of the clusters we produced radially binned spectra of the halo. Circular bins were used for MKW 4, elliptical bins with ellipticity and position angle taken from the surface brightness fits for AWM 4. All data within  $17''$  of point sources were removed and spectra were fit using an absorbed MEKAL model in a 0.4-4 keV energy band. Figure 2 shows the results of our fits.

The deprojected temperature profile for MKW 4 shows a fairly smooth decline in temperature towards the core, consistent with *ROSAT* results (Helsdon & Ponman 2000). Metal abundance is strongly affected by changes in hydrogen column. The fit quality in the central bins is poor, and we experimented with different models to fit these bins. The fits could be improved by using a two-temperature model, but the higher temperature component was never well constrained by the data. Using cooling flow models did not produce good fits except in cases where the emission from low temperature gas (*i.e.* gas at temperatures lower than  $\sim 1$  keV) was minimal.

The deprojected temperature profile for AWM 4 shows a fairly constant temperature, with a possible slight decline with increasing radius. To test whether this decline is real, we tied the four inner and two outer bins to form

Cluster	$r_{core}$ (kpc)	$\beta_{fit}$	axis ratio	position angle	amplitude	$r_{core,2}$ (kpc)	$\beta_{fit,2}$	amplitude
MKW 4	$4.44^{+0.15}_{-0.16}$	$0.447 \pm 0.001$	1.0	-	-	-	-	-
AWM 4	$96.74^{+19.13}_{-1.66}$	$0.708^{+0.054}_{-0.005}$	$1.22^{+0.04}_{-0.02}$	$174.48^{+2.39}_{-2.01}$	-	4.155	$33.58^{+20.58}_{-9.03}$	$0.998^{+0.749}_{-0.347}$

TABLE 1

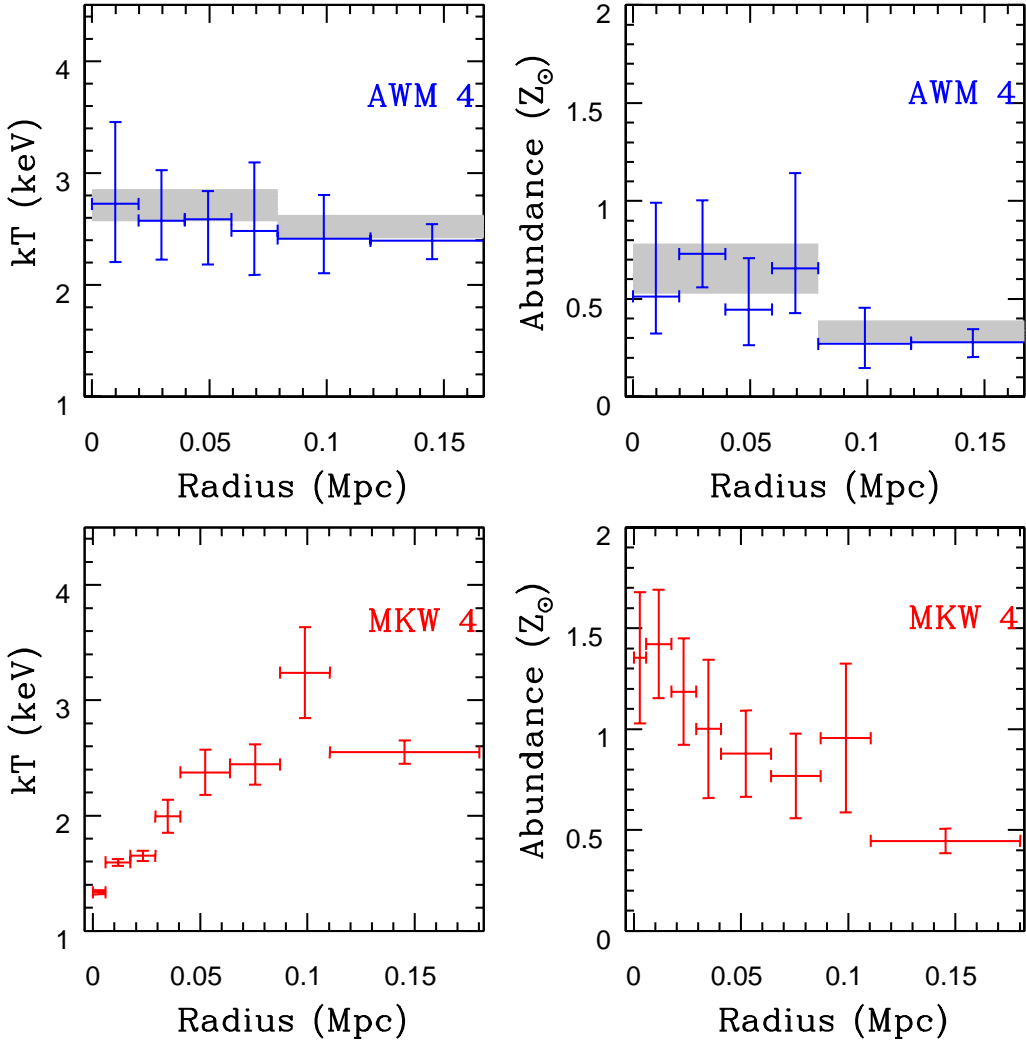


FIG. 2.— Deprojected temperature and abundance profiles of the two clusters. Symbols represent 90% error regions. Fitting was carried out using the XSPEC PROJCT model, and assuming the emission arises from an absorbed MEKAL model. Hydrogen column was fixed at the galactic value. The grey regions in the AWM 4 plots (upper panels) show fits with bins tied together to form inner and outer region. Note that the temperature difference is still not significant.

two large spectral regions. The results from these are marked as grey boxes, and show that the decrease is not statistically significant. The abundance profile shows a more marked decrease with radius. The spectra from all bins were well described by single temperature plasma models, and no more complex models were required.

For each cluster, we also investigated the abundances

of certain individual elements, using projected spectra so as to avoid reducing the quality of the data being fitted. Using the VMEKAL model in XSPEC we are able to fit Fe and Si (and in the case of MKW 4, S) individually, as well as the abundance of remaining metals and the temperature in each bin. Figure 3 shows abundance profiles for Fe, Si and S in MKW 4, shown with reference to the

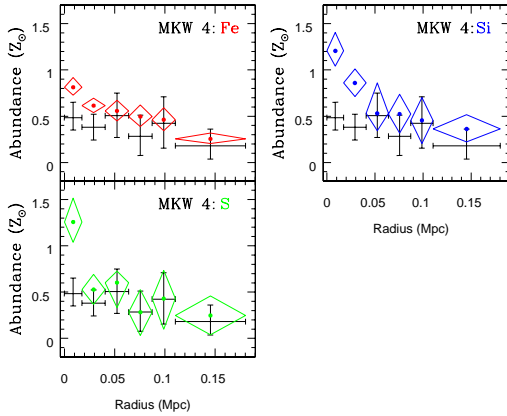


FIG. 3.— Radial abundance profiles for Fe, Si and S in MKW 4. In each plot, diamonds show the 90% error on the metal in question, as labeled on the plot. The crossed error bars show the fit to all the remaining metals, again with 90% errors.  $N_H$  was fixed at the galactic value in all fits.

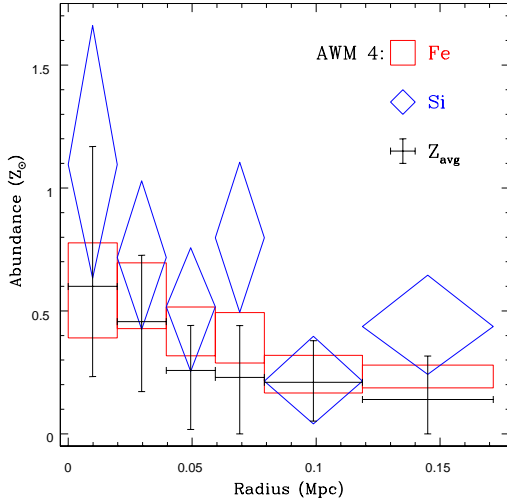


FIG. 4.— Radial abundance profiles for Fe and Si in AWM 4. Diamonds show the 90% error on Si, Boxes represent Fe and the crossed error bars show the fit to all the remaining metals, again with 90% errors.  $N_H$  was fixed at the galactic value in all fits.

profile for all other metals combined. There is a clear increase in all three elements in the core of the cluster, at the location of NGC 4073. Figure 4 shows abundance profiles for Fe and Si in AWM 4, and again shows an increase in abundance toward the core, at the location of NGC 6051.

Based on the elemental abundances of Fe and Si found in the inner bins of the two profiles, we are able to estimate the contribution made by SNIa and SNII to the enrichment of the gas in the cores of the two clusters. We assume yields of Si and Fe for type II supernovae of  $y_{Fe}=0.07 M_{\odot}$  and  $y_{Si}=0.133 M_{\odot}$  (Finoguenov et al. 2000), and from type Ia supernovae  $y_{Fe}=0.744 M_{\odot}$  and  $y_{Si}=0.158 M_{\odot}$  (Thielemann et al. 1993). For MKW 4 we estimate that  $\sim 50\%$  of the iron within 17.5 kpc of

the core was injected by SNIa. This is similar to our result for AWM 4, where we find that  $\sim 52\%$  of the iron within 49.2 kpc was injected by SNIa. However, we note that these values are strongly affected by our choice of definition of solar abundance ratios. We use the ratios of Anders & Grevesse (1989), but the more recent ratios of Grevesse & Sauval (1998) give a rather lower value for Fe/H ( $Fe/H=3.2 \times 10^{-5}$  compared to  $4.7 \times 10^{-5}$ ). This would suggest that our Fe abundances are underestimated by a factor of  $\sim 1.4$  compared to those calculated using the more recent ratios, and similarly that our estimates of SNIa contribution are lower than those we would find were we to use the Grevesse & Sauval abundances.

### 2.3. Three dimensional gas models

Using software provided by S. Helsdon, we use the surface brightness fits derived in Section 2.1 and the radial temperature profiles shown in Figure 2 to calculate quantities such as gas mass, total mass, gas cooling time and gas entropy for the inner region of each cluster. The software infers the gas density profile based on the fitted surface brightness profile and a model description of the temperature profile, and normalises it by comparison with the X-ray luminosity. Given this density profile we can use the well known equation for hydrostatic equilibrium to calculate the total mass at any given radius. Entropy is defined as  $S = T/n_e^{2/3}$ . Figure 5 shows radial profiles for these and other relevant parameters for both clusters.

Although the two clusters have quite different structures, their total mass profiles are very similar outside the core regions. This implies that the two clusters have similar total masses, with the difference in the core probably caused by the different masses of the dominant galaxies. Assuming a mass-to-light ratio for stars of  $5 M_{\odot}/L_{\odot}$ , we would expect the two galaxies to have total stellar masses of  $\sim 5 \times 10^{11} M_{\odot}$  and  $\sim 3 \times 10^{11} M_{\odot}$ , values which are comparable to the total mass of each system at 10 kpc. MKW 4 has a larger total mass and a larger mass of gas in its core regions than AWM 4. The gas fraction of AWM 4 is very low out to  $\sim 40$  kpc, where it begins to increase rapidly. In the outer regions the situation is reversed, and AWM 4 has a considerably larger gas fraction than MKW 4. MKW 4 has a relatively short cooling time in the core ( $\sim 5 \times 10^8$  yr), and the inner halo contains very low entropy gas. In AWM 4, gas entropy is significantly higher, and the cooling time is relatively long, even at very small radii. This suggests that while MKW 4 has a cool core, and may be developing towards a cooling flow, the core of AWM 4 has likely been heated. The gas fraction profile suggests that the inner halo has been 'puffed up' by the injection of energy, which is also responsible for the isothermal temperature profile.

## 3. Discussion and Conclusions

MKW 4 is similar to a number of systems observed by *Chandra* and *XMM* in that although its halo contains gas at a range of temperatures, there is no evidence of cooling below  $\sim 0.5$  keV. NGC 4636 (Xu et al. 2002), M87 (Sakelliou et al. 2002) and NGC 5044 (Tamura et al.

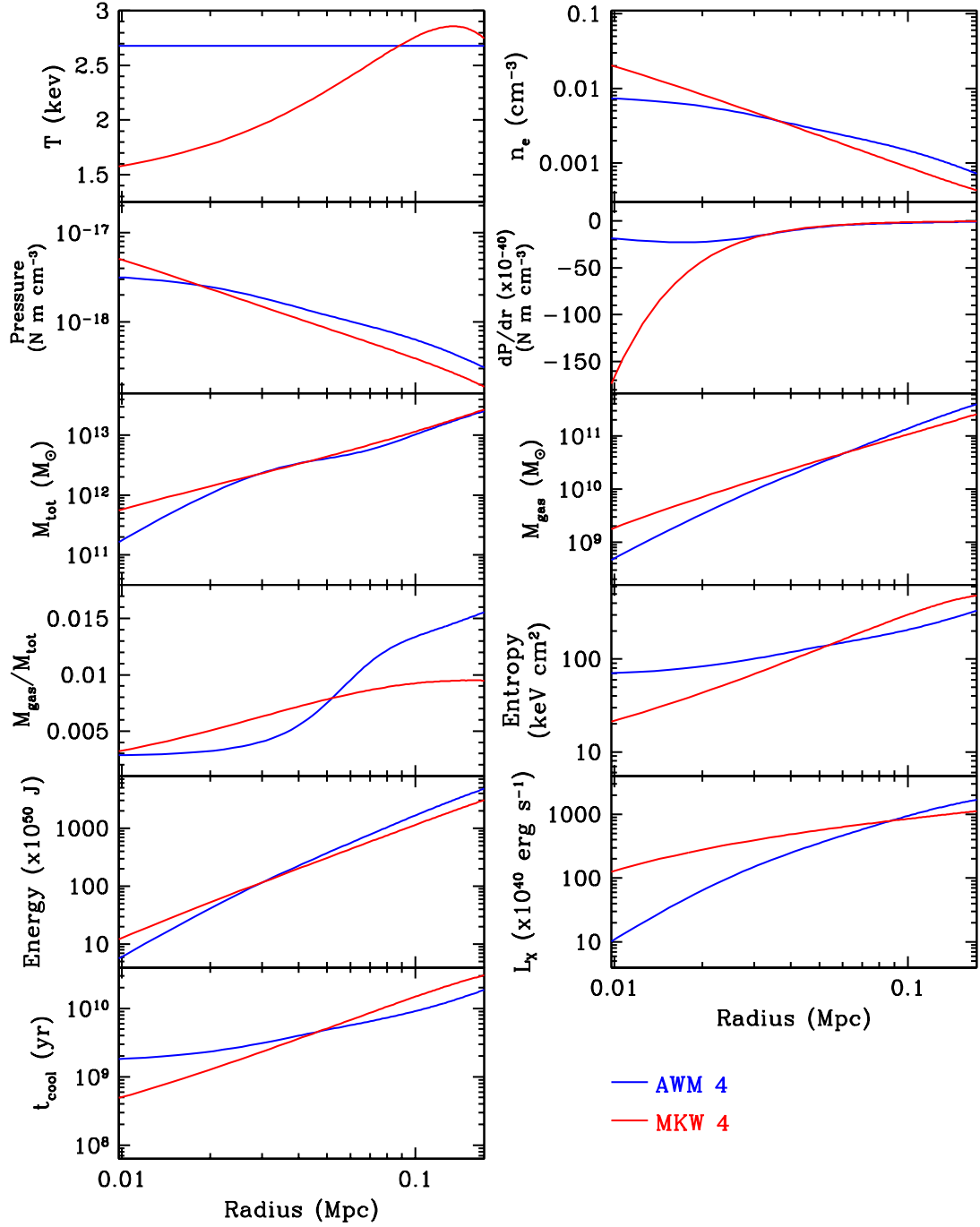


FIG. 5.— Three dimensional properties of the two clusters, as determined from their surface brightness and temperature profiles. AWM 4 is shown in blue, MKW 4 in red.

2003) all show this behaviour, with minimum temperatures of 0.5–0.6 keV. Given this minimum temperature in MKW 4, it seems likely that the halo has been heated in the past and is now in the process of cooling and re-establishing a cooling flow. This heating could have been

caused by some dynamical event, such as a sub-cluster merger, or by AGN activity.

We calculated the time required for an isothermal halo to cool to the point where its temperature profile would match that which we observe in MKW 4. In the clus-

ter core, this cooling timescale is  $\sim 200$  Myr. This is quite comparable to the activity cycle of an AGN, but very dissimilar to the spectroscopic age of the dominant galaxy. Along with the relaxed nature of the cluster, this rules out a subcluster merger as the source of heating. We therefore suggest that MKW 4 is likely to have been heated by an AGN which is currently quiescent. We also note that the temperature profile of MKW 4 is not well described by either the ‘universal’ temperature profile for relaxed clusters of Allen et al. (2001) or by models in which cooling is balanced by conduction (Voigt et al. 2002). This may support our suggestion that MKW 4 is not in a stable state and is likely to cool further.

AGN heating is also likely responsible for the isothermality of AWM 4. Taking the unlikely possibility that the isothermal temperature profile we observe is a stable, long term feature of the system, an energy input of at least  $\sim 10^{43}$  erg s $^{-1}$  is required to balance the X-ray emission from the central 100 kpc. If, as is more likely, AWM 4 once had a temperature profile much like that of MKW 4,  $\sim 9 \times 10^{58}$  erg would be needed to heat it to its current state. This is equivalent to an AGN injecting  $\sim 3 \times 10^{43}$  erg s $^{-1}$  for 100 Myr. We therefore believe that even considering efficiency factors, it is realistic to

assume AWM 4 has been heated by AGN activity.

In conclusion, we find that AWM 4 and MKW 4 are very similar systems with two major differences:

- 1. AGN activity:** While AWM 4 is currently being heated by the AGN in NGC 6051, there is no ongoing AGN activity in NGC 4073, and gas in the core of MKW 4 has been able to cool.
- 2. Galaxy mass:** NGC 6051 is considerably less massive than NGC 4073, leading to a less steeply peaked mass profile in the core of AWM 4.

The observed differences in temperature and surface brightness profile between the two systems can be explained largely through the effects of their respective central galaxies. The mass of these galaxies and the current phase of their AGN duty cycles appear to have profound effects on the structure and future evolution of the two clusters.

We are very grateful to S. Helsdon for the use of his software. This work was supported in part by NASA grants NAG5-10071 and GO2-3186X.

## References

Albert, C. E., White, R. A., & Morgan, W. W. 1977, ApJ, 211, 309  
 Allen, S. W., Fabian, A. C., Johnstone, R. M., Arnaud, K. A., & Nulsen, P. E. J. 2001, MNRAS, 322, 589  
 Anders, E. & Grevesse, N. 1989, Geo. et Cosmo. Acta, 53, 197  
 Arnaud, M., Majerowicz, S., Lumb, D., Neumann, D. M., Aghanim, N., Blanchard, A., Boer, M., Burke, D. J., Collins, C. A., Giard, M., Nevalainen, J., Nichol, R. C., Romer, A. K., & Sadat, R. 2002, A&A, 390, 27  
 Cash, W. 1979, ApJ, 228, 939  
 dell'Antonio, I. P., Geller, M. J., & Fabricant, D. G. 1995, AJ, 110, 502  
 Finoguenov, A., Arnaud, M., & David, L. P. 2001, ApJ, 555, 191  
 Finoguenov, A., David, L. P., & Ponman, T. J. 2000, ApJ, 544, 188  
 Fisher, D., Illingworth, G., & Franx, M. 1995, ApJ, 438, 539  
 Grevesse, N. & Sauval, A. J. 1998, Space Sci. Rev., 85, 161  
 Helsdon, S. F. & Ponman, T. J. 2000, MNRAS, 315, 356  
 Jansen, F., Lumb, D., Altieri, B., Clavel, J., Ehle, M., Erd, C., Gabriel, C., Guainazzi, M., Gondoin, P., Much, R., Munoz, R., Santos, M., Schartel, N., Texier, D., & Vacanti, G. 2001, A&A, 365, L1  
 Jones, C. & Forman, W. 1999, ApJ, 511, 65  
 Koranyi, D. M. & Geller, M. J. 2002, AJ, 123, 100  
 Lumb, D. 2002, <http://xmm.vilspa.esa.es/docs/documents/CAL-TN-0016-2-0.ps.gz>  
 Marty, P. B., Kneib, J. P., Sadat, R., Ebeling, H., & Smail, I. 2002, proc. SPIE, 4851, 208  
 Morgan, W. W., Kayser, S., & White, R. A. 1975, ApJ, 199, 545  
 Pratt, G. W., Arnaud, M., & Aghanim, N. 2001, in Clusters of Galaxies and the High Redshift Universe Observed in X-rays:, ed. D. M. Neumann & J. Tran Van Thanh, in press  
 Read, A. M. & Ponman, T. J. 2003, A&A, submitted  
 Sakelliou, I., Peterson, J. R., Tamura, T., Paerels, F. B. S., Kaastra, J. S., Belsole, E., Böhringer, H., Branduardi-Raymont, G., Ferrigno, C., den Herder, J. W., Kennea, J., Mushotzky, R. F., Vestrand, W. T., & Worrall, D. M. 2002, A&A, 391, 903  
 Tamura, T., Kaastra, J. S., Makishima, K., & Takahashi, I. 2003, A&A, 399, 497  
 Terlevich, A. I. & Forbes, D. A. 2002, MNRAS, 330, 547  
 Thielemann, F.-K., Nomoto, K., & Hashimoto, M. 1993, in Origin and Evolution of the Elements, ed. N. Prantzos, E. Vangioni-Flam, & M. Casse (Cambridge Univ. Press)  
 Voigt, L. M., Schmidt, R. W., Fabian, A. C., Allen, S. W., & Johnstone, R. M. 2002, MNRAS, 335, L7  
 Xu, H., Kahn, S. M., Peterson, J. R., Behar, E., Paerels, F. S. B., Mushotzky, R. F., Jernigan, J. G., & Makishima, K. 2002, ApJ, 579, 600